

Survey of $A_{LT'}$ asymmetries in semi-exclusive electron scattering on ${}^4\text{He}$ and ${}^{12}\text{C}$

D. Protopopescu,²⁴ * F. W. Hersman,²⁴ M. Holtrop,²⁴ G. Adams,³¹ P. Ambrozewicz,¹⁰ E. Anciant,² M. Anghinolfi,¹⁷ B. Asavapibhop,²³ G. Asryan,⁴⁰ G. Audit,² T. Auger,² H. Avakian,^{35, 16} H. Bagdasaryan,²⁷ J.P. Ball,¹ S. Barrow,¹¹ M. Battaglieri,¹⁷ K. Beard,²⁰ M. Bektasoglu,^{27, †} M. Bellis,³¹ N. Benmouna,¹⁴ B.L. Berman,¹⁴ W. Bertozi,²² N. Bianchi,¹⁶ A.S. Biselli,⁴ S. Boiarinov,^{19, ‡} B.E. Bonner,³² S. Bouchigny,^{18, 35} R. Bradford,⁴ D. Branford,⁹ W.J. Briscoe,¹⁴ W.K. Brooks,³⁵ V.D. Burkert,³⁵ C. Butuceanu,³⁹ J.R. Calarco,²⁴ D.S. Carman,²⁶ B. Carnahan,⁵ C. Cetina,¹⁴ S. Chen,¹¹ P.L. Cole,^{35, §} A. Coleman,^{39, ¶} D. Cords,^{35, **} P. Corvisiero,¹⁷ D. Crabb,³⁸ H. Crannell,⁵ J.P. Cummings,³¹ D. Debruyne,¹² E. De Sanctis,¹⁶ R. DeVita,¹⁷ P.V. Degtyarenko,³⁵ L. Dennis,¹¹ K.V. Dharmawardane,²⁷ K.S. Dhuga,¹⁴ C. Djalali,³⁴ G.E. Dodge,²⁷ D. Doughty,^{6, 35} P. Dragovitsch,¹¹ M. Dugger,¹ S. Dytman,²⁹ O.P. Dzyubak,³⁴ H. Egiyan,^{35, 39} K.S. Egiyan,⁴⁰ L. Elouadrhiri,^{6, 35} A. Empl,³¹ P. Eugenio,¹¹ R. Fatemi,³⁸ R.J. Feuerbach,³⁵ T.A. Forest,²⁷ H. Funsten,³⁹ G. Gavalian,^{24, 40} S. Gilad,²² G.P. Gilfoyle,³³ K.L. Giovanetti,²⁰ P. Girard,³⁴ C.I.O. Gordon,¹⁵ R.W. Gothe,³⁴ K.A. Griffioen,³⁹ M. Guidal,¹⁸ M. Guillo,³⁴ N. Guler,²⁷ L. Guo,³⁵ V. Gyurjyan,³⁵ C. Hadjidakis,¹⁸ R.S. Hakobyan,⁵ J. Hardie,^{6, 35} D. Heddle,^{6, 35} K. Hicks,²⁶ I. Hleiqawi,²⁶ J. Hu,³¹ C.E. Hyde-Wright,²⁷ W. Ingram,¹⁵ D. Ireland,¹⁵ M.M. Ito,³⁵ D. Jenkins,³⁷ K. Joo,^{7, 38} H.G. Juengst,¹⁴ J.H. Kelley,⁸ J.D. Kellie,¹⁵ M. Khandaker,²⁵ K.Y. Kim,²⁹ K. Kim,²¹ W. Kim,²¹ A. Klein,²⁷ F.J. Klein,^{35, §} A.V. Klimenko,²⁷ M. Klusman,³¹ M. Kossov,¹⁹ L.H. Kramer,^{10, 35} S.E. Kuhn,²⁷ J. Kuhn,⁴ J. Lachniet,⁴ J.M. Laget,² J. Langheinrich,³⁴ D. Lawrence,²³ T. Lee,²⁴ Ji Li,³¹ K. Livingston,¹⁵ K. Lukashin,^{35, §} J.J. Manak,³⁵ C. Marchand,² S. McAleer,¹¹ S. T. McLauchlan,¹⁵ J.W.C. McNabb,²⁸ B.A. Mecking,³⁵ J.J. Melone,¹⁵ M.D. Mestayer,³⁵ C.A. Meyer,⁴ K. Mikhailov,¹⁹ R. Minehart,³⁸ M. Mirazita,¹⁶ R. Miskimen,²³ L. Morand,² S.A. Morrow,^{2, 18} V. Muccifora,¹⁶ J. Mueller,²⁹ G.S. Mutchler,³² J. Napolitano,³¹ R. Nasseripour,¹⁰ S.O. Nelson,⁸ S. Niccolai,¹⁸ G. Niculescu,^{20, 26} I. Niculescu,^{20, 14} B.B. Niczyporuk,³⁵ R.A. Niyazov,^{35, 27} M. Nozar,³⁵ G.V. O'Rielly,¹⁴ M. Osipenko,¹⁷ A. Ostrovidov,¹¹ K. Park,²¹ E. Pasyuk,¹ G. Peterson,²³ S.A. Philips,¹⁴ N. Pivnyuk,¹⁹ D. Pocanic,³⁸ O. Pogorelko,¹⁹ E. Polli,¹⁶ S. Pozdniakov,¹⁹ B.M. Preedom,³⁴ J.W. Price,³ Y. Prok,³⁸ L.M. Qin,²⁷ B.A. Raue,^{10, 35} G. Riccardi,¹¹ G. Ricco,¹⁷ M. Ripani,¹⁷ B.G. Ritchie,¹ F. Ronchetti,^{16, 30} G. Rosner,¹⁵ P. Rossi,¹⁶ D. Rountree,²² P.D. Rubin,³³ J. Ryckebusch,¹² F. Sabatié,^{2, 27} K. Sabourov,⁸ C. Salgado,²⁵ J.P. Santoro,^{37, 35} V. Sapunenko,^{17, ‡} R.A. Schumacher,⁴ V.S. Serov,¹⁹ Y.G. Sharabian,^{40, ‡} J. Shaw,²³ S. Simionatto,¹⁴ A.V. Skabelin,²² E.S. Smith,³⁵ L.C. Smith,³⁸ D.I. Sober,⁵ M. Spraker,⁸ A. Stavinsky,¹⁹ S. Stepanyan,^{40, ††} B. E. Stokes,¹¹ P. Stoler,³¹ S. Strauch,¹⁴ M. Taiuti,¹⁷ S. Taylor,³² D.J. Tedeschi,³⁴ U. Thoma,^{13, 35} R. Thompson,²⁹ A. Tkabladze,²⁶ L. Todor,³³ C. Tur,³⁴ M. Ungaro,³¹ M.F. Vineyard,^{36, 33} A.V. Vlassov,¹⁹ K. Wang,³⁸ L.B. Weinstein,²⁷ H. Weller,⁸ D.P. Weygand,³⁵ C.S. Whisnant,^{34, ‡‡} M. Williams,⁴ E. Wolin,³⁵ M.H. Wood,³⁴ A. Yegneswaran,³⁵ J. Yun,²⁷ L. Zana,²⁴ and B. Zhang²²

(The CLAS Collaboration)

¹ Arizona State University, Tempe, Arizona 85287-1504

² CEA-Saclay, Service de Physique Nucléaire, F91191 Gif-sur-Yvette, Cedex, France

³ University of California at Los Angeles, Los Angeles, California 90095-1547

⁴ Carnegie Mellon University, Pittsburgh, Pennsylvania 15213

⁵ Catholic University of America, Washington, D.C. 20064

⁶ Christopher Newport University, Newport News, Virginia 23606

⁷ University of Connecticut, Storrs, Connecticut 06269

⁸ Duke University, Durham, North Carolina 27708-0305

⁹ Edinburgh University, Edinburgh EH9 3JZ, United Kingdom

¹⁰ Florida International University, Miami, Florida 33199

¹¹ Florida State University, Tallahassee, Florida 32306

¹² Department of Subatomic- and Radiation Physics, Ghent University, Belgium

¹³ Physikalisch Institut der Universitaet Giessen, 35392 Giessen, Germany

¹⁴ The George Washington University, Washington, DC 20052

¹⁵ University of Glasgow, Glasgow G12 8QQ, United Kingdom

¹⁶ INFN, Laboratori Nazionali di Frascati, Frascati, Italy

¹⁷ INFN, Sezione di Genova, 16146 Genova, Italy

¹⁸ Institut de Physique Nucléaire ORSAY, Orsay, France

¹⁹ Institute of Theoretical and Experimental Physics, Moscow, 117259, Russia

²⁰ James Madison University, Harrisonburg, Virginia 22807

²¹ Kyungpook National University, Daegu 702-701, South Korea

²² Massachusetts Institute of Technology, Cambridge, Massachusetts 02139-4307

²³ University of Massachusetts, Amherst, Massachusetts 01003

²⁴ University of New Hampshire, Durham, New Hampshire 03824-3568

²⁵ Norfolk State University, Norfolk, Virginia 23504

²⁶ Ohio University, Athens, Ohio 45701
²⁷ Old Dominion University, Norfolk, Virginia 23529
²⁸ Penn State University, University Park, Pennsylvania 16802, USA
²⁹ University of Pittsburgh, Pittsburgh, Pennsylvania 15260
³⁰ Universita' di ROMA III, 00146 Roma, Italy
³¹ Rensselaer Polytechnic Institute, Troy, New York 12180-3590
³² Rice University, Houston, Texas 77005-1892
³³ University of Richmond, Richmond, Virginia 23173
³⁴ University of South Carolina, Columbia, South Carolina 29208
³⁵ Thomas Jefferson National Accelerator Facility, Newport News, Virginia 23606
³⁶ Union College, Schenectady, NY 12308
³⁷ Virginia Polytechnic Institute and State University, Blacksburg, Virginia 24061-0435
³⁸ University of Virginia, Charlottesville, Virginia 22901
³⁹ College of William and Mary, Williamsburg, Virginia 23187-8795
⁴⁰ Yerevan Physics Institute, 375036 Yerevan, Armenia

(Dated: September 17, 2019)

Single spin azimuthal asymmetries $A_{LT'}$ were measured at Jefferson Lab using 2.2 and 4.4 GeV longitudinally polarized electrons incident on ${}^4\text{He}$ and ${}^{12}\text{C}$ targets in the CLAS detector. $A_{LT'}$ is related to the imaginary part of the longitudinal-transverse interference and in quasifree nucleon knockout it provides an unambiguous signature for final state interactions (FSI). Experimental values of $A_{LT'}$ were found to be below 5%, typically $|A_{LT'}| \leq 3\%$ for data with good statistical precision. Optical Model in Eikonal Approximation (OMEA) and Relativistic Multiple-Scattering Glauber Approximation (RMSGA) calculations are shown to be consistent with the measured asymmetries.

PACS numbers: 24.70.+s, 25.30.Dh, 27.10.+h

Keywords: helicity asymmetry; CLAS

I. INTRODUCTION

Although quasielastic ($\omega \approx Q^2/2m_p$) ($e, e'p$) reactions have been a well-used tool for the study of nuclear structure [1, 2, 3, 4, 5], gaps in our understanding of this reaction still persist. One of the most remarkable open questions at present is how many effective nucleons there are in nuclear single particle orbitals (i.e. what are the spectroscopic factors), and whether this number does indeed change with Q^2 , as suggested in Lapikas et al. [6]. Fissum et al. [7] argue that the present data are not strong enough to support Lapikas' conclusions, so further study of this issue will be required. One important ingredient in these analyzes is a thorough understanding of final state interactions (FSI).

Understanding FSI is also a crucial ingredient in being able to understand short-range correlations in nuclei [8], effects such as the transition to a quark-gluon picture

at higher Q^2 , and nuclear transparency [6]. It is also important in testing the predictions of perturbative QCD and understanding dense nuclear matter.

There are numerous approaches to FSI: distorted wave impulse approximation (DWIA), the eikonal approximation, Glauber theory, etc. [9], but exact calculations are only possible for $A \leq 3$ at low momentum. The effects of FSI must therefore be measured experimentally, but they cannot be isolated directly in a cross-section measurement. They can only be identified through their interference with the dominant process, i.e. by separating the interference terms of the polarized cross-section [10]. This is now possible following the commissioning of reliable, high-current polarized sources at facilities such as Mainz, MIT-Bates, NIKHEF and TJNAF.

The beam helicity asymmetry $A_{LT'}$ turns out to be the ideal observable for the study of FSI. In general, $A_{LT'}$ corresponds to the imaginary part of the longitudinal-transverse interference component of the hadron tensor and it vanishes whenever the reaction proceeds through a channel with a single dominant phase [11, 12]. Indeed, in the plane wave impulse approximation (PWIA) where the rescattering is ignored and the hadron tensor is real and symmetric, $A_{LT'}$ is zero.

In quasifree proton knockout, $A_{LT'}$ is almost entirely due to the interference of the two dominant channels: direct knockout and rescattering through FSI. Because $A_{LT'}$ is much less sensitive to other effects such as meson-exchange currents (MEC), it is considered the best observable for monitoring rescattering effects in knockout reactions [13].

*Electronic address: protopop@jlab.org; Present affiliation: University of Glasgow, Glasgow G12 8QQ, United Kingdom

[†]Current address: Ohio University, Athens, Ohio 45701

[‡]Current address: Thomas Jefferson National Accelerator Facility, Newport News, Virginia 23606

[§]Current address: Catholic University of America, Washington, D.C. 20064

[¶]Current address: Systems Planning and Analysis, Alexandria, Virginia 22311

^{**}Deceased

^{††}Current address: Old Dominion University, Norfolk, Virginia 23529

^{‡‡}Current address: James Madison University, Harrisonburg, Virginia 22807

A measurement of $A_{LT'}$ requires a polarized electron beam. When polarized beam is used, the differential cross-section contains two terms [10]: a helicity-independent term Σ and a helicity-dependent term $h\Delta$, with h standing for the electron helicity $h = \pm 1$. They can be separated in the helicity asymmetry $A_{LT'}$ defined as

$$A_{LT'} = \frac{d\sigma^+ - d\sigma^-}{d\sigma^+ + d\sigma^-} = \frac{\Delta}{\Sigma} \quad (1)$$

and measured by simply flipping the beam helicity. In this formula, the $d\sigma^+$ and $d\sigma^-$ denote differential cross-sections corresponding to the $+1$ and -1 helicities, respectively. Practical advantages of extracting this observable are that detector efficiencies cancel out in the ratio and that spectroscopic factors are not required for comparison with theory.

Two previous measurements of $A_{LT'}$ on ^{12}C were carried out at MIT-Bates by Mandeville et al. [3] and Jiang et al. [14]. However, while the data were seen to be consistent with DWIA, they were too limited to draw further conclusions. More data, with higher statistical accuracy, are necessary to differentiate among the models. To date, no measurements of $A_{LT'}$ in ^4He have been done although theoretical predictions have been made by Laget [15]. ^4He is interesting because, despite being a four-body system, it is a high density nucleus. A comprehensive analysis of FSI effects in ^4He will provide good insight into the significance of these effects in heavier nuclei.

This article presents a survey of $A_{LT'}$ asymmetries in $(\vec{e}, e'p)$ reactions on ^{12}C and ^4He in the quasielastic regime, exploring kinematics not previously accessible. The questions addressed are: what is the strength of the asymmetry signal and whether present models can describe qualitatively and/or quantitatively the measurements. The theoretical models used herein were proven to successfully reproduce the L , T and LT components of the cross-section [9], but their accuracy in describing the LT' term has not yet been tested.

II. KINEMATIC VARIABLES AND RESPONSE FUNCTIONS

Electron scattering in the one-photon-exchange approximation (OPEA) is schematically shown in Fig. 1. An electron of initial energy E_e and momentum \mathbf{k} scatters through an angle θ_e to a final energy E'_e and momentum \mathbf{k}' . The reaction plane is rotated by an angle ϕ_{pq} relative to the scattering plane. The target nucleus is denoted by A and the undetected recoiling system by B . The ejected proton is detected in coincidence with the scattered electron e' . The coordinate system is chosen so that the z -axis lies along the momentum transfer \mathbf{q} and the y -axis is perpendicular to the scattering plane, parallel to $\mathbf{k} \times \mathbf{k}'$. For Q^2 we use the convention $Q^2 = -q_\nu q^\nu \geq 0$, where q is the four-momentum of the virtual photon.

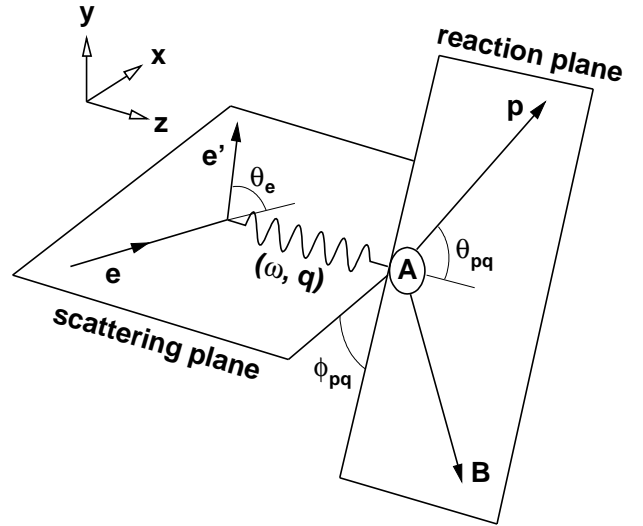


FIG. 1: Kinematics for the semi-exclusive $A(\vec{e}, e'p)B$ reaction.

The missing energy E_m and momentum \mathbf{p}_m for this semi-exclusive channel can be reconstructed as:

$$E_m = \omega - T_p - T_r, \quad \mathbf{p}_m = \mathbf{q} - \mathbf{p}, \quad (2)$$

where $\mathbf{q} = \mathbf{k} - \mathbf{k}'$ and $\omega = E_e - E'_e$ are the momentum and energy transferred by the electron, respectively, T_p is the kinetic energy of the outgoing proton and T_r is the kinetic energy of the recoiling system (see Fig. 1).

In the absence of detected initial or final hadronic-state polarization, the cross-section for polarized electron scattering in the laboratory frame can be expressed as [10]:

$$\begin{aligned} \frac{d^5\sigma}{dE'_e d\Omega_e d\Omega_p} = & K\sigma_M(v_T f_T + v_L f_L) & (3) \\ & + v_{TT} f_{TT} \cos 2\phi_{pq} \\ & + v_{LT} f_{LT} \cos \phi_{pq} \\ & + h v_{LT'} f_{LT'} \sin \phi_{pq} \end{aligned}$$

where σ_M is the Mott cross section and K includes the phase-space and recoil factors. In the ultra-relativistic limit, the electron helicity states $h = +1$ and $h = -1$ correspond to spin parallel and antiparallel to \mathbf{k} , respectively.

The labels L and T refer to the longitudinal and transverse components of the virtual photon polarization and therefore correspond to the electromagnetic current components with respect to the direction of \mathbf{q} . Double subscripts indicate interference terms. The coefficients v_i ($i = T, L, TT, LT$ and LT') are known functions of the electron kinematics. The response functions f_i are proportional to bilinear combinations of the nuclear current matrix elements and contain all of the nuclear structure information.

From equations (1) and (3), the single spin asymmetry $A_{LT'}(\phi_{pq})$ can be written as:

$$A_{LT'}(\phi_{pq}) = v_{LT'}f_{LT'}\sin\phi_{pq}/[f_d + v_{TT}f_{TT}\cos 2\phi_{pq} + v_{LT}f_{LT}\cos\phi_{pq}], \quad (4)$$

where $f_d = v_T f_T + v_L f_L$ denotes the ϕ -independent term.

III. EXPERIMENT

The data were taken during the e2a period between April 15 and May 27, 1999 in Hall B at Jefferson Laboratory using polarized electron beams of energy $E = 2.261$ GeV and $E = 4.461$ GeV at beam currents of $2 - 10$ nA.

The electron beam at CEBAF was produced by a strained GaAs crystal optically pumped by circularly polarized laser light [16]. This setup permits the rapid flipping of the sign of the electron helicity. Helicity pulses were associated in pairs of opposite helicity and the leading pulse helicity was chosen by a pseudo-random number generator in order to eliminate helicity-correlated fluctuations. The electron polarization was determined by frequent Møller polarimeter measurements to be $\langle P_B \rangle = 0.63 \pm 0.02(\text{stat.}) \pm 0.03(\text{syst.})$. The polarization measurements and the helicity decoding procedure are described in [17].

The ^{12}C target was a $1 \times 1 \text{ cm}^2$ plate of 1 mm thickness and density $\rho_C = 1.786 \text{ g/cm}^3$. The helium target consisted of liquid ^4He ($\rho_{He} = 0.139 \text{ g/cm}^3$) contained in a cylindrical aluminium cell. Two cells were used during our data taking: 1) 4.99 cm long and 0.97 cm in diameter and 2) 3.72 cm long and 2.77 cm in diameter.

Final state particles were detected in the CEBAF Large Acceptance Spectrometer (CLAS) which is described in detail in [18]. CLAS consists of a superconducting toroidal magnet and drift chambers to reconstruct the momenta of the tracks of charged particles between 8° and 142° in polar angle and with roughly 80% azimuthal coverage. It has gas Cherenkov counters (CC) for electron identification, scintillation counters for measurement of the time-of-flight (TOF) and electromagnetic calorimeters (EC) to identify showering particles such as electrons and photons. The trigger was formed by fast coincidences between the CC and EC at 2.261 GeV and by EC alone at 4.461 GeV. Data were taken at an acquisition rate of approximately 2.2 kHz and an average (nucleon) luminosity during the run of $\mathcal{L} = 7 \times 10^{33} \text{ s}^{-1}\text{cm}^{-2}$.

IV. DATA REDUCTION AND ANALYSIS

Data were acquired with the CLAS “single electron trigger” configuration described above. Further improvements in the electron identification were performed off line, where the total energy deposited in EC was used

to identify electrons and eliminate background such as negative pions. Protons were identified by time-of-flight. The reconstructed electron and proton vertex coordinates were used to eliminate events originating in the windows and temperature shield of the liquid-target cells. Electron momentum corrections were applied to compensate for drift chamber misalignments and uncertainties in the magnetic field mapping. These corrections were in the range of 1–3%.

With CLAS, it is customary to use software fiducial cuts to exclude regions of non-uniform detector response. However, we will show later on in this paper how these detector responses cancel out in the ratio Eq. (1). For that reason no fiducial cuts are deemed necessary for the present analysis. Also, since the statistics are low and integration over a relatively large missing energy range is employed, we considered it unnecessary to apply radiative corrections on the data. The systematic error introduced by this omission was estimated to be below 2%.

Data recorded during the run [29] amounted to 323 M triggers at 2.261 GeV and 346 M triggers at 4.461 GeV for carbon, and 310 M triggers at 2.261 GeV and 442 M triggers at 4.461 GeV for helium. After data reduction and the quasielastic cut described below, the statistics corresponding to the two beam settings were 3.8 M and 0.3 M for carbon, respectively, and 2.7 M and 0.25 M for helium, respectively.

The quasielastic (QE) kinematics region was selected by a cut along the quasielastic ridge $\omega = Q^2/2m_p + \Delta E$ with the condition $\omega_1 < \omega < \omega_2$ and limits given by the equation:

$$\omega_{1,2} = (1/2 \pm \xi)Q^2/m_p + \Delta E, \quad (5)$$

where $\xi = 0.2$ sets the width of our cut and ΔE is a shift due to the momentum dependence of the nucleus-nucleon potential, taken to be equal to 0.03 GeV. This cut is roughly equivalent to $0.7 < x_B < 1.6$, where x_B is the Bjorken variable. In conjunction with (5) we rejected events with $E_m > 0.1$ GeV to reduce the contribution of multi-particle final states.

The Q^2 coverage of the selected data was $0.35 - 1.80 \text{ GeV}^2/\text{c}^2$ at 2.261 GeV beam energy and $0.80 - 2.40 \text{ GeV}^2/\text{c}^2$ at 4.461 GeV. For the study of the quasielastic regime we divided the kinematics explored into four Q^2 bins, nine p_m bins and sixty ϕ_{pq} bins. The cut from (5) is applied for each case so that in practice we work with 4-dimensional bins in coordinates Q^2 , p_m , ω and ϕ_{pq} .

For the investigation of the missing energy dependence of $A_{LT'}$ outside the quasielastic regime, we used 0.1 GeV bins in E_m and we integrated over Q^2 while splitting p_m into two large bins. Consequently, we worked with 3-dimensional bins in coordinates E_m , p_m and ϕ_{pq} .

To measure the beam helicity asymmetry defined in Eq. (1) we calculated the ratio

$$A_m = \frac{N^+ - N^-}{N^+ + N^-}, \quad (6)$$

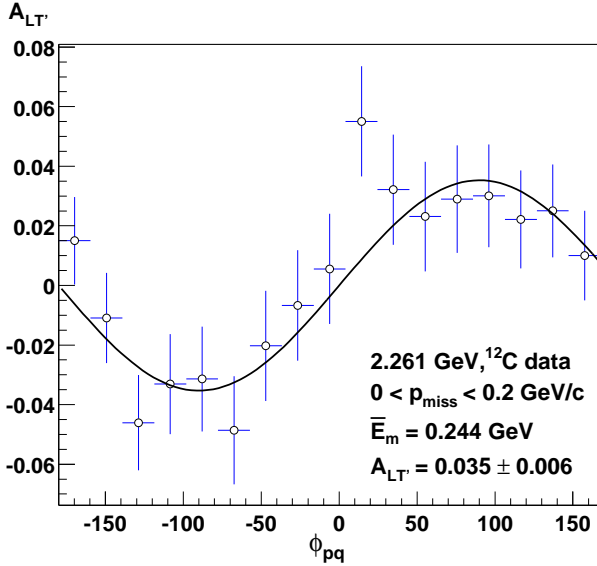


FIG. 2: (Color online) Fit using function Eq. (7): ^{12}C data at 2.261 GeV are integrated over all Q^2 and over missing momentum in the interval $0 < p_m < 0.2 \text{ GeV}/c$ (see Fig. 5.e). For clarity, the number of bins is reduced here and the asymmetry is corrected for beam polarization using Eq. 9.

where N^+ and N^- are, respectively, the number of $(e, e'p)$ events with positive and negative helicity within the chosen kinematic bin.

False asymmetries were investigated by assigning helicities randomly to each event and comparing the resulting A_m^{random} asymmetry with zero. The false asymmetry values were much smaller than the statistical errors.

The yields N^+ and N^- from (6) were corrected for beam charge asymmetry (BCA). Since the BCA corrections are extracted from inclusive data, the systematic uncertainty introduced by this procedure is approximately 1% of the statistical error on N^\pm [19].

This procedure described in the previous paragraph was repeated for all 60 bins in ϕ_{pq} . Then these values were used to extract A_{exp} by fitting the ϕ_{pq} dependence with the one-parameter function:

$$A_m(\phi_{pq}) = A_{\text{exp}} \sin \phi_{pq}, \quad (7)$$

The TT and LT contributions were neglected in this fit but the systematic uncertainty introduced by this approximation was estimated to be below 5% [19]. A fit with function (7) is shown in Fig. 2.

For small measured asymmetries the statistical uncertainty on $A_m(\phi_{pq})$ from (6) was dominated by the $1/N$ dependence (where $N = N^+ + N^-$):

$$\delta A_m(\phi_{pq}) \approx \sqrt{(1 - A_m^2(\phi_{pq}))/N} \approx 1/\sqrt{N}, \quad (8)$$

The MINUIT [20] fit uncertainty for A_{exp} dominated the statistical uncertainty on $A_m(\phi_{pq})$, which was in the range of $\pm 20\%$.

To account for the partial polarization of the incident beam, the extracted asymmetry A_{exp} was scaled by the beam polarization P_B to obtain the true asymmetry $A_{LT'}$:

$$A_{LT'} = A_{\text{exp}}/P_B, \quad (9)$$

The beam polarization was measured with a relative uncertainty of less than 5%. This, added in quadrature to the other sources of systematic errors mentioned before (radiative effects, BCA and choice of fit function), yield a systematic error $< 8\%$. Thus, the data presented herein is dominated by the fit uncertainty which is the only one shown on the plots.

V. THEORETICAL CALCULATIONS

The experimental results are compared with theoretical models developed by the Ghent group [9, 21, 22]. Both models employ bound-state wavefunctions calculated within the context of a mean-field approximation to the $\sigma - \omega$ model [23, 24]. In all calculations, the Γ_{cc2} hadronic current operator and the Coulomb gauge were used and the spectroscopic factors for ^{12}C were set equal to $S = 2j + 1$. The electron distortion - i.e. the distortion of the electron wave function in the Coulomb field of the nucleus - has been neglected, since its effect for nuclei as light as ^4He and ^{12}C is very small. All calculations presented here are relativistic and include the spinor distortion [30] of the lower components in the bound-state wave function due to the scalar and vector potential of the $\sigma - \omega$ model.

The Optical Model in the Eikonal Approximation (OMEA) is based on the relativistic eikonal approximation for the ejectile scattering wave function and a relativistic mean-field approximation to the Walecka model [25]. The optical potential used in the OMEA calculations is EDAIC, of Cooper *et al.* [26]. The only basic difference between OMEA and the traditional distorted-wave impulse approximation (DWIA) [13] is the use of the eikonal approximation to construct the scattering wave function in OMEA. While in DWIA the exact solutions to the equations determining the scattering wave function are used, the OMEA adopts the approximate eikonal solutions to the same equation [9]. The eikonal solution approaches the exact one if the missing momentum of the ejectile is sufficiently small in comparison with the momentum transfer q .

An extension of the eikonal method is introduced to cope with high proton kinetic energies ($T_p \geq 1 \text{ GeV}$) where the elementary proton-nucleon scattering becomes highly inelastic and the use of optical potentials is no longer the natural choice for describing final-state interactions. The Relativistic Multiple-Scattering Glauber Approximation (RMSGA) is a relativistic generalization of the Glauber approach described in [27]. Whereas the optical potential approaches model the FSI effects through estimating the loss of flux from elastic

proton-**nucleus** data, Glauber approaches rely on elastic proton-**nucleon** data. The Glauber model is an A -body multiple-scattering theory, which relies in addition to the eikonal on the so-called frozen approximation. This requires the spectator nucleons to be stationary during the time that the projectile travels through the target nucleus.

We investigate here missing momenta up to 0.6 GeV/c. However, we would like to note that, as illustrated by the measurements of Liyanage *et al.* [5], at missing momenta above 0.3 GeV/c it is very likely that more complicated reaction mechanisms (channel coupling, two-nucleon knockout, etc.) come into play and can contribute by up to 50% of the cross-section [7]. Comparisons between theory and data above $p_m = 0.3$ GeV/c should be viewed in this context. Addressing the question of many-body effects is beyond the scope of this paper.

VI. ACCEPTANCE AND BIN AVERAGING EFFECTS

Bin averaging effects are not negligible when summing over relatively wide kinematics. This was a concern in the case of our Q^2 and ω coordinates (see section IV) since the bins are 0.36 to 0.40 GeV $^2/c^2$ wide in Q^2 and about 50 MeV in ω . These widths were chosen in order to keep the statistical errors reasonably small, but then the theory calculations must account for the resulting bin averaging, as described in the following.

Let us consider an arbitrary bin B_n of width $\Delta\chi = \Delta Q^2 \Delta\omega \Delta p_m \Delta\phi_{pq}$ and denote by $\langle\chi\rangle_n$ its center of weight. Let us observe that the r.h.s. of Eq. (6) can be put in the form below:

$$A_m(\langle\chi\rangle_n) = \frac{\sum_{k=1}^K (N_k^+ - N_k^-)}{\sum_{k'=1}^K (N_{k'}^+ + N_{k'}^-)} \equiv \frac{\sum_{k=1}^K \sigma_k^h \epsilon_k}{\sum_{k'=1}^K \sigma_{k'}^0 \epsilon_{k'}}, \quad (10)$$

where we formally divided the $\omega \times Q^2$ subspace within bin B_n into K sub-bins and denoted by ϵ_k the (unknown) detector acceptance within sub-bin b_k . We used the shorthand notations $\sigma^h = \sigma^+ - \sigma^-$ and $\sigma^0 = \sigma^+ + \sigma^-$ for the polarized and unpolarized parts of the total cross-section, respectively.

After some manipulation, Eq. (10) can be written as

$$\begin{aligned} A_m(\langle\chi\rangle_n) &= \sum_{k=1}^K \left(\frac{\sigma_k^h}{\sigma_k^0} \right) \left(\frac{\sigma_k^0 \epsilon_k}{\sum_{k'=1}^K \sigma_{k'}^0 \epsilon_{k'}} \right) \\ &\equiv \sum_{k=1}^K A_m(\langle\chi\rangle_k) w_k, \end{aligned} \quad (11)$$

where we separated the weights w_k defined as

$$w_k = \frac{\sigma_k^0 \epsilon_k}{\sum_{k'=1}^K \sigma_{k'}^0 \epsilon_{k'}} = \frac{N_k}{N}, \quad N = N^+ + N^-, \quad (12)$$

which can be easily calculated using the experimental yields. Then theory calculations can be done for each k sub-bin and added up within B_n , i.e.

$$A_t(\langle\chi\rangle_n) = \sum_{k=1}^K A_c(\langle\chi\rangle_k) w_k, \quad (13)$$

where $A_c(\langle\chi\rangle_k)$ are pure model calculations for the kinematics $\langle\chi\rangle_k$.

To determine the optimal number of sub-bins, K , a compromise was sought between a small number that minimizes both the statistical error on w_k and the computational time, and a large number that better compensates for kinematic averaging. The value fulfilling these conditions was found to be $K = 4$ with negligible statistical error on w_k [19].

Smooth theoretical curves are obtained by cubic spline interpolation of the $A_t(\langle\chi\rangle_n)$ array.

VII. RESULTS

Two variations of the $A_{LT'}$ asymmetry are presented: **A)** the missing momentum dependence at quasielastic kinematics with $E_m < 0.1$ GeV and **B)** the missing energy dependence up to $E_m = 0.9$ GeV. Theoretical calculations accompany the missing momentum plots.

The ${}^4\text{He}$ data is consistent with zero except for a possible small positive region at missing momentum around $0.15 < p_m < 0.3$ at $Q^2 < 1.4$ GeV. The ${}^{12}\text{C}$ 2.262 GeV data are negative for $0.1 < p_m < 0.2$ and become mostly consistent with zero for missing momenta above 0.3 GeV and for all p_m range at 4.462 GeV.

A. Missing momentum dependence

The dependence of $A_{LT'}$ at quasielastic kinematics as a function of p_m is presented in Fig. 3–4. The data were divided into four Q^2 bins for each beam energy setting. There is a direct mapping between θ_{pq} and p_m , such that low p_m corresponds to low θ_{pq} . The equivalent angular range covered by the mentioned plots would be $0^\circ < \theta_{pq} < 27^\circ$.

The ${}^{12}\text{C}$ data are accompanied by OMEA calculations at all kinematics and by RMSGA calculations in the range $|\mathbf{q}| > 1$ GeV/c, where the latter model is applicable. The ${}^4\text{He}$ data is compared with RMSGA only. The error bars shown on the data are fit uncertainties as explained in section IV.

A first observation is that measured asymmetries are very small at low p_m . This is to be expected as low

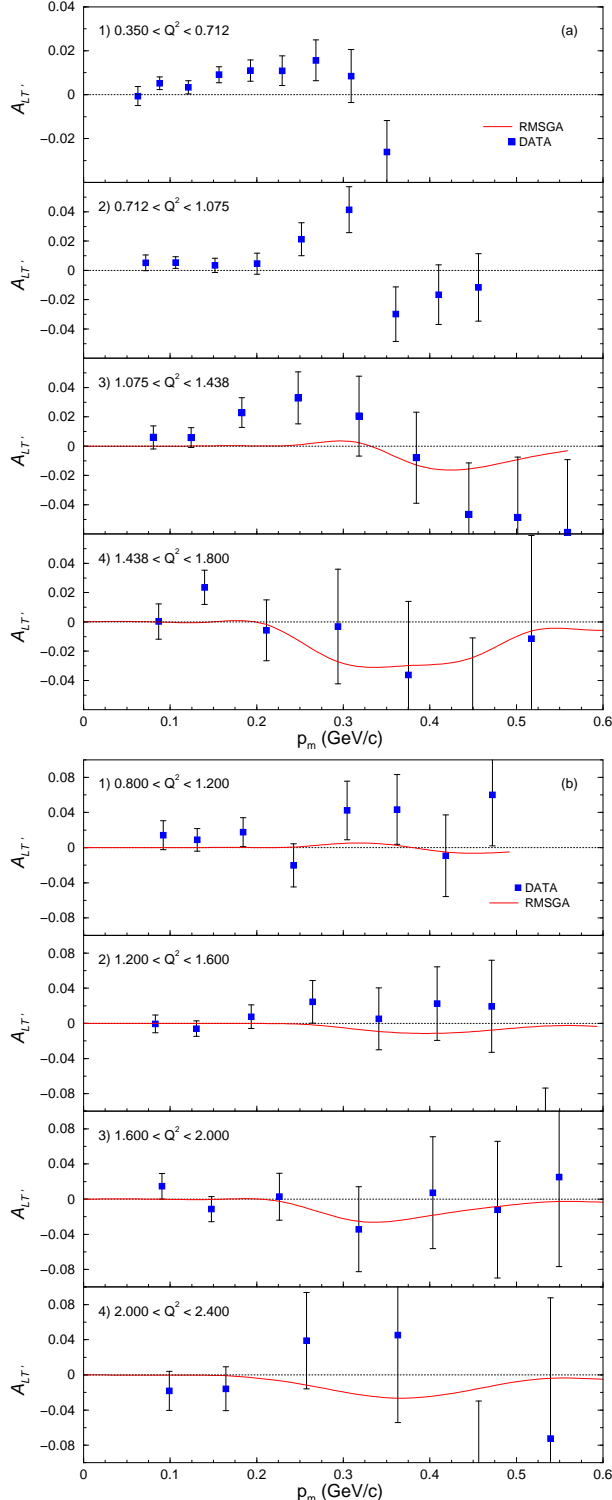


FIG. 3: (Color online) Dependence of $A_{LT'}$ versus missing momentum p_m for ${}^4\text{He}(e, e'p)$ at (a) $E = 2.262$ GeV and (b) $E = 4.462$ GeV, in four Q^2 bins along the quasielastic ridge. The curves correspond to RMSGA calculations used as described in section VI. Error bars are statistical.

p_m corresponds to low θ_{pq} where the helicity asymme-

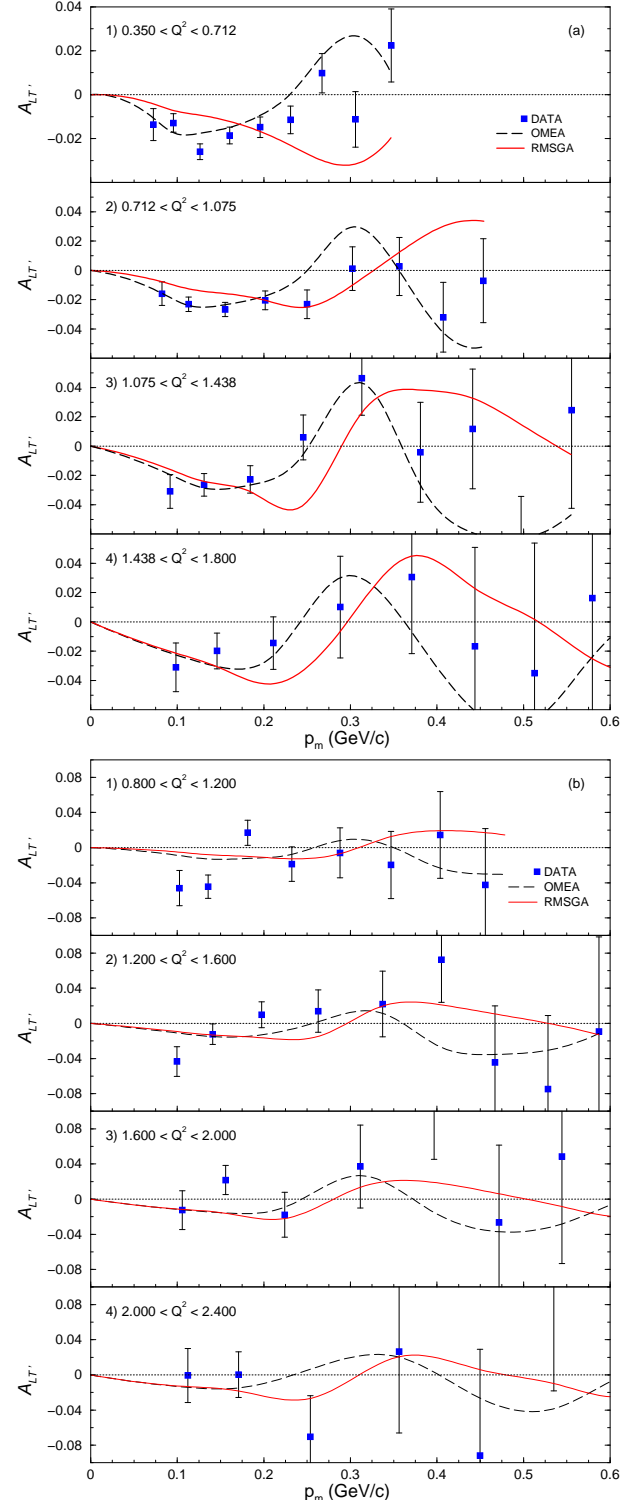


FIG. 4: (Color online) Dependence of $A_{LT'}$ versus missing momentum p_m for ${}^{12}\text{C}(e, e'p)$ at (a) $E = 2.262$ GeV and (b) $E = 4.462$ GeV, in four Q^2 bins along the quasielastic ridge. The curves correspond to RMSGA (solid) and OMEA (dotted) calculations used as described in section VI. Error bars are statistical.

try vanishes with the phase-space: $A_{LT'} \sim \sin \theta_{pq}$. The sharp rise of $A_{LT'}$ at low missing momentum shown by the low Q^2 calculations from [4] is at our energy setting seen neither in the measurement nor in the calculations shown herein. There are at least two reasons for the smaller asymmetries here: a) at higher energy the effects of FSI are smaller and the calculation would naturally produce a smaller oscillation in $A_{LT'}$ and b) in the case of ^{12}C cancellation between unresolved $1s$ and $1p$ contributions significantly reduces the inclusive asymmetry.

The overall aspect of the plots is almost independent of Q^2 . This is an important point to note when integrating over Q^2 in the next subsection.

Although the statistical significance is not remarkably high, the 2.262 GeV data suggest a structure between $0.1 < p_m < 0.3$ GeV/c. Its position appears to not vary much with Q^2 and, in the case of ^{12}C , both models more or less reproduce this feature.

The large change in slope seen on the ^{12}C calculations at $p_m \approx 0.3$ GeV/c is likely due to the dip in the $1s_{1/2}$ and $1p_{3/2}$ momentum distributions at slightly higher p_m as calculated in [27]. This effect, attributed to bound-nucleon and ejectile spinor distortion [7], is shifted to lower missing momenta and partially washed out by the FSI. The difference between the two calculations is due to the fact that RMSGA will locate the effect at higher p_m compared with OMEA, reflecting the fact that the predicted effect of FSI on the observables is smaller in Glauber approaches than in optical potential-based models.

Although carbon data (Fig. 4) benefit from higher statistical precision than the helium data, separation of the s and p shells in ^{12}C is not possible due to the limited energy resolution of CLAS. The interplay between the two shells is important, since our calculations showed that the s - and p -shell contributions are of opposite sign [19, 28]. The effect of the s -shell can be visualized by comparing the 2.262 GeV helium and carbon plots: both targets feature the mentioned structure between $0.1 < p_m < 0.3$ GeV/c. But while the ^4He asymmetry stays positive in this missing momentum range, the ^{12}C asymmetry goes through negative values, most likely due to the interplay between the two shell components.

B. Missing energy dependence

The missing energy dependence of $A_{LT'}$ was further studied over a range spanning up to $E_m \leq 0.8$ GeV. The plots are shown in figures 5 (a–h). The very first point on all the plots corresponds to the valence knockout kinematics, investigated in the previous subsection, but integrated over a larger p_m interval (see figure caption).

In accordance with the s -shell effect mentioned in subsection VII A, the lowest E_m sample point shows negative asymmetries for ^{12}C compared with positive asymmetries in the case of ^4He (Fig. 5, plots a and e).

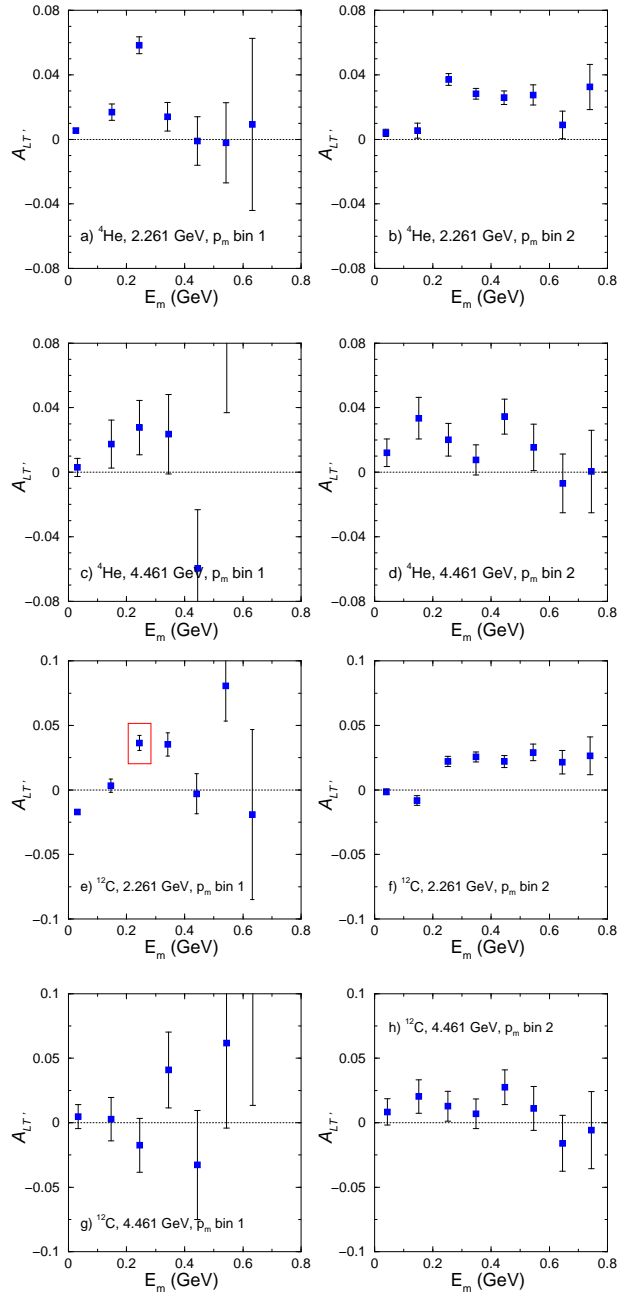


FIG. 5: (Color online) $A_{LT'}$ versus E_m for helium (plots a–d) and carbon (plots e–h). The two missing momentum bins are defined as follows: 1) $0 < p_m < 0.2$ and 2) $0.2 < p_m < 0.45$ with p_m in GeV/c. The E_m bins are 0.1 GeV wide. No radiative corrections were applied. Error bars are statistical. The boxed point on plot e was extracted from the sinusoid presented in Fig. 2.

There is a clear and dramatic increase in $A_{LT'}$ at $E_m = 0.25$ GeV where the pion production channel opens. It is very likely that this extra channel interferes with the other open channels to produce a larger $A_{LT'}$. This feature is less pronounced at higher p_m since here other processes besides direct knockout and pion pro-

duction are smearing the interference peak.

Theoretical calculations at higher missing energy to accompany these data would be valuable.

VIII. SUMMARY

We have measured the $A_{LT'}$ asymmetry in quasielastic ($\omega \approx Q^2/2m_p$) reactions on ^{12}C and ^4He in order to determine the contribution of final state interactions in the one-proton knockout reaction.

Overall, the measured asymmetries in the quasielastic region were below 5%, typically in the range of 0-3% for data with good statistics. This seems to indicate that FSI are very small and unimportant for these light nuclei at these energy settings. Nevertheless, the results presented herein confirm the presence of asymmetry signals in $(\vec{e}, e' p)$ data and complement the (scarce) world data on this subject. Our survey could indicate the regions of interest for future investigations, such as $p_m \geq 0.3$ GeV/c or higher missing energies, for which in this paper the calculations either differ or were unavailable, and the statistics used were relatively scarce.

While areas of disagreement were observed, all models showed qualitative agreement with the experiment. A detailed comparison with theory for ^{12}C would require

separation of major shells, since they are predicted to contribute with opposite sign to the asymmetry. Within the range of validity of the models and summing over the final states, one can assert that the theoretically modeled FSI are consistent with the experiment.

Acknowledgments

The authors would like to thank R. Owens for interesting discussions and useful suggestions. We would like to acknowledge the outstanding efforts of the staff of the Accelerator and the Physics Divisions at JLab that made this experiment possible.

This work was supported in part by the Instituto Nazionale di Fisica Nucleare, the French Centre National de la Recherche Scientifique, the French Commissariat à l'Energie Atomique, the U.S. Department of Energy, the National Science Foundation, Emmy Noether grant from the Deutsche Forschungsgemeinschaft, the Korean Science and Engineering Foundation and the UK's Engineering and Physical Sciences Research Council. The Southeastern Universities Research Association (SURA) operates the Thomas Jefferson National Accelerator Facility for the United States Department of Energy under contract DE-AC05-84ER40150.

[1] S. Frullani and J. Mougey, *Adv. Nucl. Phys.* **14**, 1 (1984).
[2] J. J. Kelly, *Adv. Nucl. Phys.* **23**, 75 (1996).
[3] J. Mandeville et al., *Phys. Rev. Lett.* **72**, 3325 (1994).
[4] S. M. Dolfini et al., *Phys. Rev.* **C60**, 064622 (1999).
[5] N. Liyanage et al., *Phys. Rev. Lett.* **86**, 5670 (2001), see also J. Gao et al., *Phys. Rev. Lett.* **84**, 3265 (2000).
[6] L. Lapikas, G. van der Steenhoven, L. Frankfurt, M. Strikman, and M. Zhalov, *Phys. Rev.* **C61**, 064325 (2000).
[7] K. G. Fissum et al., in press (2004), nucl-ex/0401021.
[8] B. Zhang, Ph.D. thesis, MIT, USA (2003).
[9] D. Debruyne, J. Ryckebusch, S. Janssen, and T. Van Cauteren, *Phys. Lett.* **B527**, 62 (2002).
[10] T. W. Donnelly and A. S. Raskin, *Ann. Phys.* **2** (1986).
[11] S. Boffi, C. Giusti, and F. D. Pacati, *Nucl. Phys.* **A435**, 697 (1985).
[12] G. Co, A. M. Lallena, and T. W. Donnelly, *Nucl. Phys.* **A469**, 684 (1987).
[13] S. Boffi, C. Giusti, F. D. Pacati, and M. Radici, *Electromagnetic Response of Atomic Nuclei* (Oxford University Press, 1996).
[14] X. Jiang, Ph.D. thesis, MIT, Boston, USA (1998).
[15] J.-M. Laget, *Nucl. Phys.* **A579**, 333 (1994).
[16] C. K. Sinclair et al., *Tech. Rep. CEBAF-PR-89-002*, CEBAF (1989).
[17] D. Protopopescu et al., *Tech. Rep. CLAS-ANALYSIS 2002-105*, TJNAF (2002).
[18] B. A. Mecking et al., *Nucl. Instr. Meth.* **A503**, 513 (2003).
[19] D. Protopopescu, Ph.D. thesis, University of New Hampshire, USA (2002), abridged version published as D. Protopopescu et al., *CLAS-ANALYSIS 2003-101*, TJNAF (2003).
[20] *MINUIT 95.03*, CERN, cern library d506 ed. (1995).
[21] D. Debruyne, Ph.D. thesis, Ghent University, Ghent, Belgium (2001).
[22] D. Debruyne and J. Ryckebusch, *Nucl. Phys.* **A699**, 65 (2002).
[23] C. Horowitz and B. Serot, *Nucl. Phys.* **A368**, 503 (1981).
[24] B. Serot and J. Walecka, *Adv. Nucl. Phys.* **191**, 1 (1986).
[25] D. Debruyne, J. Ryckebusch, W. Van Nespen, and S. Janssen, *Phys. Rev.* **C62**, 024611 (2000).
[26] E. Cooper, S. Hama, B. Clark, and R. Mercer, *Phys. Rev.* **C47**, 297 (1993).
[27] J. Ryckebusch et al., *Nucl. Phys.* **A728**, 226 (2003).
[28] J. J. Kelly, *private communication*.
[29] CLAS torus magnet current was set at 2500 A
[30] Spinor distortion : The lower (i.e. small) components in the Dirac wave functions for the nucleons take on the following form $(\sigma \cdot \mathbf{p})/(E + M + S(r) - V(r)) \times (\text{radial wave function})$. By "spinor distortion" one refers to the presence of the term " $S(r) - V(r)$ ", where $S(r)$ is the scalar and $V(r)$ the vector part of the "mean-field" potential.